Available online at www.sciencedirect.com
ScienceDirect
Proceedings of the Combustion Institute 33 (2011) 533–540
Proceedings of the Combustion Institute
www.elsevier.com/locate/proci

Evidence of aliphatics in nascent soot particles in premixed ethylene flames

Jeremy P. Cain [a], Joaquin Camacho [a], Denis J. Phares [a], Hai Wang [a,*], Alexander Laskin [b,**]

[a] Department of Aerospace and Mechanical Engineering, University of Southern California, Los Angeles, CA 90089, USA
[b] William R. Wiley Environmental Molecular Sciences Laboratory, Pacific Northwest National Laboratory, P.O. Box 999, MSIN K8-88, Richland, WA 99352, USA

Abstract

Chemical composition of nascent soot in burner-stabilized, premixed ethylene–oxygen–argon flames was studied using micro-FT-IR spectroscopy. The flames have an identical unburned gas composition with equivalence ratio equal to 2.07, but they differ in cold gas velocity. Nascent soot was sampled using a dilution probe over a range of burner surface-to-probe separation. The particles were deposited on thin-film substrates in a cascade impactor at two cut sizes of $D_{50} = 10$ and 56 nm. The micro-FT-IR spectra revealed the presence of aliphatic C–H, aromatic C–H and a number of oxygenated functionalities. Spectral analyses were made to quantify variations of the aliphatic and aromatic C–H groups with flame temperature and sampling position. Results show that the aliphatic-to-aromatic C–H ratio is greater than unity in all cases, indicating the presence of an appreciable amount of aliphatic C–H bonds in nascent soot. The relative content of aliphatic components was found to increase with an increase in the maximum flame temperature. To examine the nature of these aliphatic constituents, a thermal desorption–chemical ionization time-of-flight mass spectrometry was used to softly fragment a soot sample and ionize the fragments. Results suggest that the aliphatic constituents are alkylated aromatics with molecular weights spanning from 200 to 900 amu. This work provides definitive and quantitative observations that aliphatics are abundant at early stages of soot mass and size growth.

Keywords: Soot; Premixed flame; Chemical composition; Particle size distribution; FT-IR

1. Introduction

Mature soot particles are fractal aggregates of nearly spherical primary particles 20–50 nm in diameter. These primary particles are composed of large polycyclic aromatic hydrocarbons (PAHs) arranged in a turbostratic fashion [1]. Mature soot typically has a carbon-to-hydrogen atomic ratio ranging from 8:1 to 12:1 [2]. Recent studies suggest that nascent soot undergoing mass and size growth can be drastically different from mature soot. Like the precursor soot discussed by Dobbins and coworkers [3,4], these particles can have compositions and internal structures different from one another, depending on their time,

* Corresponding author. Fax: +1 213 740 8071.
** Corresponding author. Fax: +1 509 371 6139.
E-mail addresses: haiw@usc.edu (H. Wang), alexander.laskin@pnl.gov (A. Laskin).

1540-7489/$ - see front matter © 2010 The Combustion Institute. Published by Elsevier Inc. All rights reserved.
doi:10.1016/j.proci.2010.06.164

temperature, and gas-phase composition history [5–9]. Moreover, nascent soot particles <10 nm in diameter appear to be liquid-like [10–12]. Transmission electron microscope (TEM) and atomic force microscope (AFM) images show that they form flattened [10–13] or crater-like structures [11] upon impact with a substrate. Results obtained by TEM, Small Angle Neutron Scattering (SANS) and other techniques suggest that nascent soot has a C/H atomic ratio as small as unity and a mass density of approximately 1.5 g/cm^3 [10], which is notably smaller than that of mature soot (1.8–2.0 g/cm^3) [14].

Using photoionization mass spectrometry (PIAMS), Öktem et al. [15] suggested that soot extracted in the post-flame region of a premixed, flat ethylene flame contains large amounts of aliphatic components in addition to stabilomer PAHs with peak intensities around coronene. The presence of aliphatics in nascent soot is thought to be consistent with its liquid-like behavior [10,16], as well-carbonized soot is expected to be rigid and retain its sphericity upon impact. More recently, Maricq [17] used laser ablation particle mass spectrometry to probe the composition of nascent soot online, and Bouvier et al. [18] used laser desorption/laser ionization mass spectrometry to probe soot generated from lightly sooting premixed flames. Both studies show stabilomer PAHs to be the dominant aromatic constituent of soot. What remains unresolved is whether aliphatic components are present and their concentrations relative to the aromatic components. Neither Maricq [17] nor Bouvier et al. [18] found conclusive evidence supporting the existence of aliphatic compounds. Unlike the approach of Öktem et al. [15], in which soft evaporation and photoionization were used to probe the particle material, the laser ablation techniques employed by Maricq [17] and Bouvier et al. [18] are probably too destructive and, thus, insensitive to aliphatics.

In comparison, FT-IR spectroscopy has the advantage of probing soot chemistry nondestructively. It allows for the determination of the nature and content of various functional groups, including aliphatic and aromatic C–H bonds, and oxygenated functionalities. Although several previous studies (e.g., [19–21]) have used this method to analyze soot generated from a wide array of fuels and conditions, no quantitative comparison between these functional groups had been made until recently. Using an FT-IR spectrometer coupled to a microscope (micro-FT-IR), we [22] examined the composition of soot sampled in the post-flame region ($\geqslant$1.0 cm from the burner surface) of several well-studied ethylene–argon–oxygen flames. Results show that soot with particle sizes ranging from 10 to 100 nm has aliphatic-to-aromatic C–H ratios exceeding 10 for all particle sizes, which is in agreement with the results of Öktem et al. [15]. Based on a recent Raman spectroscopy study [23], these groups are most likely to be bound to the soot surfaces as alkyl or alkenyl functionalities.

The aforementioned observation impacts several fundamental assumptions in soot formation models. In general, present models assume that the surface of nascent, growing soot is aromatic in nature and mass growth follows the aromatic hydrogen-abstraction–carbon-addition (HACA) mechanism [24–26]. The presence of aliphatic hydrogen on soot surfaces affect not only physical properties (e.g., mass density and reactive site density), it should also influence the surface reaction chemistry and possibly particle–particle coagulation behavior. A quantitative speciation of chemical composition, especially during the early stage of soot formation, is critical to the further advancement of available soot models [16].

The present study extends the application of micro-FT-IR to smaller burner-to-probe separations (H_p) with the goal of determining the relative concentrations of functional groups in soot during its early stage of mass and size growth. We report size and spatially-resolved micro-FT-IR analyses of nascent soot in a set of ethylene flames at an equivalence ratio of 2.07. As in the earlier study [22], we utilized a probe sampling technique [27–29] coupled to a cascade impactor to collect soot samples without having to dissolve them in a solvent. This technique eliminates the past problem where only soluble components could be analyzed [19–21] by the FT-IR technique. The aliphatic-to-aromatic C–H, carbonyl [C=O]-to-aromatic C–H and [C–O]-to-aromatic C–H ratios were determined as a function of flame temperature and H_p position. The results show that aliphatic components are abundant at early stages of soot mass and size growth. We also utilized a thermal desorption–chemical ionization time-of-flight mass spectrometer (TD-CITOF-MS) to examine the molecular constituents of nascent soot particles. Aspects of this instrument have been discussed in Ref. [30]. The combined micro-FT-IR and TD-CITOFMS results indicate that aliphatic C–H in soot is attributable to alkylated aromatics having molecular weights ranging from 200 to 900 amu.

2. Experimental

The experimental setup shown schematically in Fig. 1 has been discussed in detail elsewhere [22]. Briefly, the setup includes a flat flame burner 7.62 cm in diameter, an *in situ* sample probe [11,27,29], a nano-scanning mobility particle sizer (nano-SMPS, TSI 3085) and a cascade impactor (MSP, nano-MOUDI II, 125B). The flame from a mixture containing 16.3% (mol) ethylene (Matheson, 99.99%), 23.7% (mol) oxygen (Air Liquide,

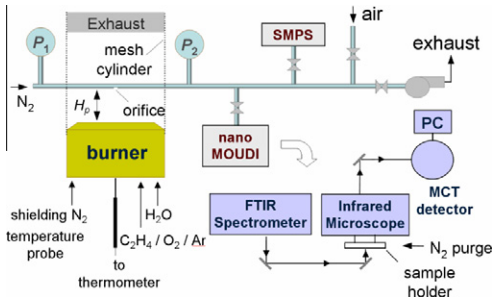

Fig. 1. Schematics of experimental setup.

99.993%) and 60% (mol) argon (Oxarc, 99.98%) (equivalence ratio $\phi = 2.07$) was stabilized on a water-cooled burner. A 4.17 L/min (STP) sheath flow of dry nitrogen surrounds the flame, and a stainless steel mesh screen surrounds the burner to minimize flame perturbations.

Dry nitrogen flows through the sample probe to dilute the particles entering the probe through a 500 μm diameter pinhole [22]. The pressure gradient inside the tube is controlled and the pressure at the pinhole determines the sample dilution ratio [11]. Particle size was characterized by a nano-SMPS [31] placed downstream of the pinhole. A micro-orifice uniform deposition impactor (MOUDI) [32,33] without stage rotation was used for particle sampling. The sampling substrates were 200 μm thick, 5.0 mm square silicone frame windows holding 150 nm thin-film of Si_3N_4 (Silson, Ltd.). Soot was collected on stages 13 and 10, which have aerodynamic cut diameters of $D_{50} = 10$ and 56 nm, respectively. The dilution ratio for MOUDI sampling was ~300 [22]. Copper tubing was used between the sample probe and MOUDI.

A Bruker IFS 66/S FT-IR spectrometer coupled to an optical microscope (micro-FT-IR) was used in this study. The substrate with impacted soot sample was placed in an environmental stage (Linkam, FT-IR 600), and a home-made N_2 purge cell rested atop the stage [34] to reduce CO_2 and H_2O vapor presence in the IR beam path. FT-IR spectra were collected in double sided, forward–backward mode with a KBr beamsplitter, using Mertz phase correction, Norton-Beer (medium) apodization function and a zero filling factor of 2. An average of fifteen spectra, each 512 co-added scans, was taken for each sample and blanks at a spectral resolution of 4 cm^{-1}. Acquisition of each spectrum takes roughly 30 min. Quantitative analysis of functional groups was accomplished by calibrating the absorption peaks using a set of standards [22].

A recently developed TD-CITOF-MS instrument [30] was used to analyze the vapor of a soot sample. The vapor is produced by thermal desorption upon heating a filament on which the soot was deposited. The sample was collected thermophoretically by rapid insertion of a nichrome coil into the flame at ~1 cm above the burner surface. Particles were desorbed under N_2 at 10 Torr and a filament temperature of 700 °C. The sample vapor passes through a CI region where a strip of 0.5 mCi of Americium-241 initiates the gas-phase ionization chemistry and the sample molecules are subsequently ionized by proton transfer from H_3O^+ ions. The CI chamber is maintained below 10 Torr to minimize formation of cluster ions. Ions are then focused into a vacuum chamber ($<10^{-6}$ Torr) using a series of electrostatic lenses, while the neutral gas is skimmed away in a one-stage evacuation region. A mass spectrum of the ions is obtained by orthogonal extraction time-of-flight mass spectrometry. The mass resolution, given as the full-width at half height, is $(m/z)/500$ and the detection range is $m/z < 1000$. A 10 kHz pulse produced by a function generator (Agilent model 33220A) triggers a high voltage pulser (HV Pulse Technologies) for repeated rapid application of an electric field orthogonal to the initial ion trajectory. Ions are accelerated towards an electrostatic reflector, which reflects the ions towards a microchannel plate detector (Burle). The function generator simultaneously triggers a time-to-digital converter (Ortec model 9353) to monitor the current pulses produced when individual ions impact the detector.

A set of four canonical flames reported earlier [11] were studied: flames C3–C6. They have the same stoichiometry but differ in cold gas velocity, with the maximum flame temperature $T_f = 1610$ (C6), 1660 (C5), 1710 (C4) and 1736 ± 50 K (C3), measured by a 150 μm thin-wire thermocouple and corrected for radiation. The cold gas velocities are 8.0, 6.5, 5.5 and 4.5 cm/s (STP), respectively. Particles were sampled over H_p value ranging from 0.4 to 0.95 cm at a 0.05 cm interval. Thus, FT-IR spectroscopy was performed on 96 samples spanning the experimental conditions of four flames, two stages and 12 H_p values.

3. Results and discussion

A typical baseline-corrected, smoothed FT-IR spectrum is shown in Fig. 2. All of the absorption peaks and their assignments are summarized in Table 1. Aromatic C–H stretch is observed at 3050 cm^{-1}, with aliphatic C–H vibrational modes at lower wavenumbers: 2960, 2920, 2860 and 2820 cm^{-1}. Two other C–H vibrations are attributed to unsaturated C–H (=CH_2) at 1460 cm^{-1} and acetylenic C–H at 3300 cm^{-1}. Carbonyl C=O, along with the C–C stretch enhanced by the presence of carbonyl, are observed at 1720 and 1600 cm^{-1}, respectively. Singly bonded oxygen (to carbon) is seen as ether C–O–C stretch (1260 cm^{-1}), C–O stretch in esters, ethers, alcohol,

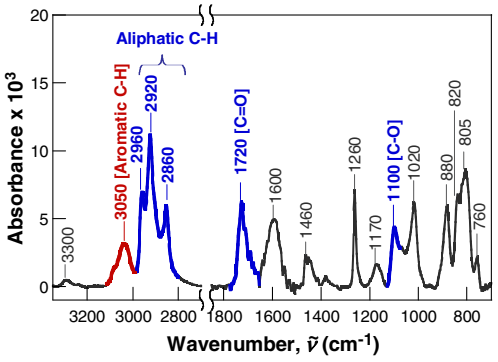

Fig. 2. Typical FT-IR spectrum of a soot sample.

and phenol (1100 cm^{-1}), and unsaturated hydroxyl C–C–O stretch (1020 cm^{-1}).

The distribution of soot particle sizes deposited on the nano-MOUDI stages is the product of the particle size distribution function (PSDF) $dN/d\log D_m$, where N is the number density and D_m is the particle diameter, and stage collection efficiency η. It should be noted that η is a function of aerodynamic diameter, whereas the SMPS particle size distribution function is based on mobility diameter D_m. A TEM investigation [35] using soot deposited in a cascade impactor, however, shows the two values to be approximately the same above ~50 nm. Below around 20 nm, the two sizes are again expected to be roughly the same, based on a consideration of available theoretical evidence [36,37]. A plot of $(dN/d\log D_m/N)$ and weighted by collection efficiency η is displayed in Fig. 3 for all four flames at three H_p values. The size distribution was obtained with the mobility analyzer using a dilution ratio of 300. For both stages, the size distribution of deposited particles shifts to smaller sizes as the flame temperature increases. For example, stage 13 has a mass

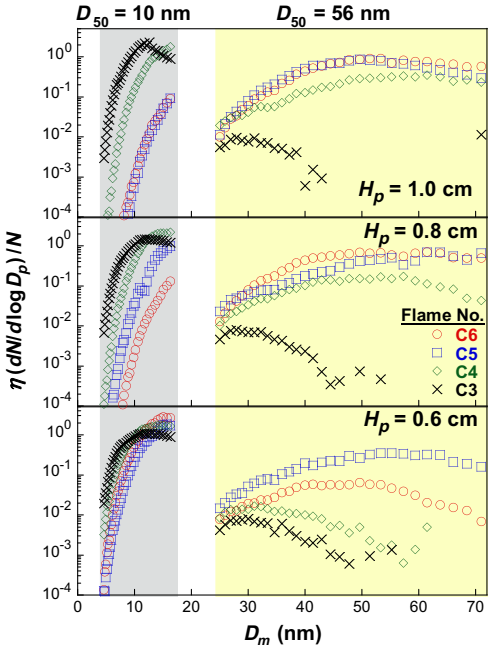

Fig. 3. Estimated distribution of particle sizes deposited on the nano-MOUDI stages 13 ($D_{50} = 10$ nm) and 10 ($D_{50} = 56$ nm).

median diameter of ~15 nm in flame C6 and ~10 nm in flame C3, while that for stage 10 is ~55 nm in flame C6 and ~30 nm in C3. These rather complex behaviors are attributable to the differences in the bimodal soot PSDFs observed in these flames in the past [11,38].

Quantitative analyses of aromatic C–H (3050 cm^{-1}), aliphatic C–H (2960, 2920, 2860, 2820 cm^{-1}), C=O (1720 cm^{-1}) and C–O (1100, 1020 cm^{-1}) functionalities were made through a set of calibration standards. Molar absorptivities

Table 1
IR peaks observed for soot samples.

Peak (cm^{-1})	Assignment	References
3300	Acetylenic C–H stretch	[19,20]
3050	Aromatic C–H stretch	[5,6,19,20]
2960	Alkane CH_3 asymmetric stretch	[5,6,19,20]
2920	Alkane CH_2 asymmetric stretch	
2860	Alkane CH_3 symmetric stretch	
2820	Alkane CH_2 symmetric stretch	
1720	Carbonyl C=O	[19,20]
1600	Aromatic C=C enhanced by C=O conjugation	[19]
1460	Unsaturated C–H (=CH_2) stretch	[19,20]
1380	C–H plane deformation (CH_2)	[19,20]
1260	Ether C–O–C stretch	[19]
1100	C–O stretch in ethers, esters, alcohol, and phenol	[19,20]
1020	Unsaturated hydroxyl C–C–O stretch	[19,20]
880	Substituted aromatic C–H	[19,20]
820	Undetermined	[19,20]
805	Undetermined	
760	Substituted aromatic C–H	[19,20]

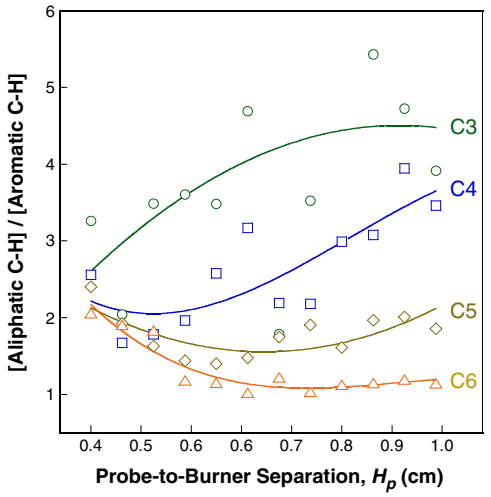

Fig. 4. Aliphatic-to-aromatic C–H concentration ratios determined for particles with $D_{50} = 10$ nm as a function of probe-to-burner separation. Symbols are experimental data; lines are drawn to guide the eye.

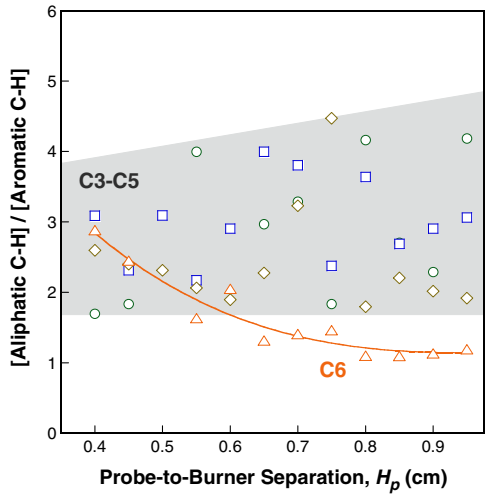

Fig. 5. Ratios of aliphatic-to-aromatic C–H concentrations determined for particles with $D_{50} = 56$ nm as a function of probe-to-burner separations. Symbols are experimental data; lines are drawn to guide the eye. The shaded area represents the cluster of data for flames C3 and C5 (see text).

relative to aromatic C–H are 1.6 for aliphatic C–H, 16 for C=O and 5.4 for C–O groups [22]. Fig. 4 shows the aliphatic-to-aromatic C–H ratio of soot samples with $D_{50} = 10$ nm as a function of probe-to-burner separation distance (H_p) in a range of 0.4–0.95 cm. Three important observations may be made. First, the aliphatic-to-aromatic C–H ratio is greater than unity in all cases, indicating aliphatics are abundant in the soot samples. This is in agreement with Öktem et al. [15], who used PIAMS – a method independent of the current technique. Second, the aliphatic content is influenced by the flame temperature: the presence of aliphatics increase towards higher flame temperatures. Third, the aliphatic-to-aromatic C–H ratio varies spatially; and this variation is dependent on the flame temperature (see Fig. 5).

Measurements taken over the H_p values near the flame front ($H_p = 0.4$–0.6 cm) reveal a fall-then-rise behavior in the aliphatic-to-aromatic C–H ratio for the lower temperature flames C6 and C5. It is possible that the spatial variation for small burner-to-probe separations, as seen in Fig. 4, is caused by probe effects, as discussed in detail in a recent work [38]. Specifically, we concluded that the probe acts as a flow stagnation surface, causing the local axial flow velocity and gas temperature to drop just ahead of the sampling point. For experiments conducted at $H_p < 0.6$ cm, the maximum flame temperature would be determined by the probe instead of the heat flux into the flat flame burner. Under this condition the variation in the aliphatic-to-aromatic C–H ratio should diminish as H_p decreases. Figure 4 shows that this is indeed the case; the aliphatic-to-aromatic C–H ratios measured for all flames converge to a value between 2 and 3 at $H_p = 0.4$ cm. Hence, the results obtained for lower H_p values are perhaps less indicative of the effect of the maximum flame temperature and more indicative of the probe effect.

For larger particles, i.e., those collected on stage 10 ($D_{50} = 56$ nm), the spatial dependency weakens; the aliphatic-to-aromatic C–H ratios for flames C3, C4 and C5 scatter between ~2 and 4. Only flame C6 shows a definite fall in the aliphatic-to-aromatic C–H ratio at higher H_p values. The loss of spatial sensitivity is probably the results of particle–particle coagulation in the probe coupled with experimental uncertainty. As we discussed earlier, the dilution ratio employed is around 300 (optimized for the FT-IR sensitivity), which is smaller than the value traditionally used in our study of PSDFs. Particle–particle coagulation does occur in the sampling line at this dilution ratio [22]. The net effect results in averaging the chemical composition over a range of particles with different original sizes.

Additionally, data reproducibility remains somewhat low. The scatters seen in Figs. 3 and 4 for the aliphatic-to-aromatic C–H ratios are around 50% of the data value. These scatters are attributable to three factors: signal averaging, baseline correction and peak deconvolution. Nonetheless, these experimental uncertainties do not affect the major conclusion about the abundance of aliphatics in the soot samples analyzed.

As discussed earlier, the flame temperature has a strong impact on the aliphatic-to-aromatic C–H

ratio. To emphasize this effect, Fig. 6 shows this ratio as a function of T_f at three representative H_p values of 0.6, 0.8 and 0.95 cm. Since the flame sheet is located ~0.2 cm above the burner surface and the probe perturbation occurs within 0.3 cm from the probe surface [38], the probe should have a minimal effect on the maximum flame temperature; and the T_f values shown in the figure is the same or nearly the same as the true flame temperature. Again, the results highlight that the aliphatic-to-aromatic C–H ratio increases with an increase in the flame temperature. Furthermore, this ratio can be quite large, with values measured up to 10. Figure 6 also shows C–O and C═O concentrations relative to that of aromatic C–H. Like aliphatic C–H, the relative abundances of the oxygenated groups increase with an increase in the flame temperature, though the values are much smaller. The abundance of the functional groups

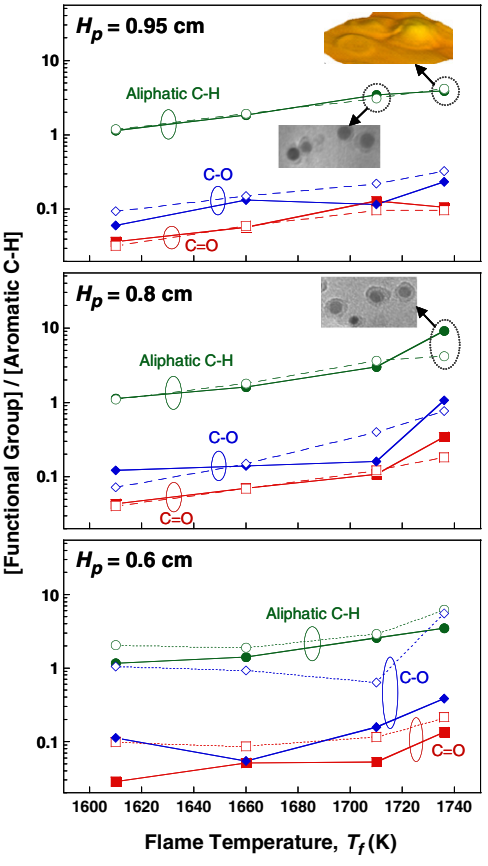

Fig. 6. Concentration ratios of various functional groups determined for particles with $D_{50} = 10$ nm (closed symbols) and $D_{50} = 56$ nm (open symbols) as a function of the maximum flame temperature, determined in the present work. Lines are drawn to guide the eye. The TEM and AFM micrographs in top and middle panels are taken from Ref. [11].

follows the following order, as observed in the post-flame region previously [22]: [C═O] < [C–O] « [aliphatic C–H].

The effect of probe perturbation requires some further considerations. The probe causes flow stagnation, leading to a longer residence time in the chemically reacting flow before particles are sampled. It also causes the gas temperature to drop. These effects were observed within a ~0.3 cm thick boundary layer adjacent to the probe surface [27,38]. While we cannot rule out the possibility that all of the observed aliphatics are the result of soot surface reactions with gaseous aliphatic molecules in the boundary layer, this possibility is quite unlikely considering experimental evidence available from previous studies. First, as shown in the top and middle panels of Fig. 6, images of particles sampled thermophoretically show spreading on the substrate surface, which can be expected only if the particles were wax- or liquid-like, a property characteristic of paraffinic compounds. Second, assuming that the PAH units in nascent soot are of the size of coronene [15,17], using the molecular weight of coronene (300 g/mol) and aliphatic-to-aromatic C–H ratio of 5 (representative of our results), we estimate the atomic C/H ratio to be approximately unity. This estimate is quite insensitive to the assumption made about the nature of the aliphatics and their chain length. A C/H atomic ratio of unity is in close agreement with results for nascent soot in similar flames obtained using the non-intrusive, SANS method [10]. In the SANS study it was determined that the atomic C/H ratio in nascent soot must be around unity and the particle mass density ≈ 1.5 g/cm^3 in order to reconcile the data measured using several techniques.

Lastly, we discuss the nature of the aliphatic constituents in nascent soot. PIAMS studies showed a range of C_2–C_8 alkenes upon fragmentation of a soot sample [15]. These probably originated from saturated or unsaturated aliphatic side chains covalently bound to the aromatic units. Desorption of a soot sample even softer than PIAMS along with a chemical ionization technique would preserve the alkyl side chains on the aromatics. Under this condition, we expect to observe a broad range of higher masses without seeing an abundant amount of small, aliphatic masses. The TD-CITOF-MS technique shows that this is indeed the case. The soot sample was fragmented by heating the substrate to 700 °C. Mass spectra were taken continuously during thermal desorption. Figure 7 shows a typical TD-CITOF-MS spectrum of a soot sample collected from flame C3 by thermophoretic sampling. The spectrum shown here was taken after approximately 20 min of heating. Very few ions (other than H_3O^+ cluster ions) were observed below $m/z = 100$. Rather, a broad range of ions spanning from 100 to 900 amu was observed. Compared to

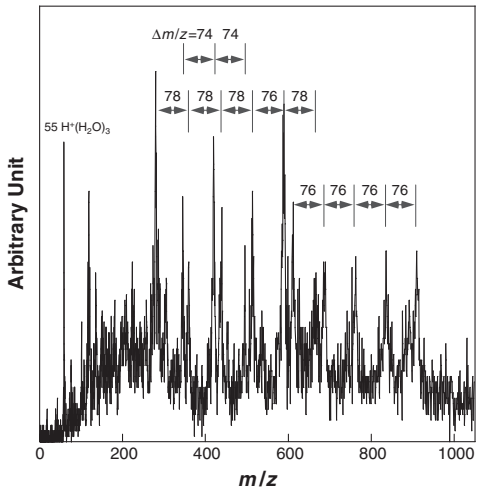

Fig. 7. TD-CITOF-MS spectrum of nascent soot collected in flame C3 at around 1.0 cm from the burner surface.

PIAMS results, the TD-CITOF-MS spectrum shows a lesser number of prominent PAH stabilomers, as expected from the fact that they are alkylated. In fact, what appears to be the background noises in the mass range of 200–1000 is mostly various alkylated PAH stabilomers. Nonetheless, the separation of prominent peaks is approximately a few Daltons greater than 72, as shown in the figure, which is six times the atomic weight of carbon, indicating that the dominant structural units remain to be aromatic in nascent soot, despite the presences of a large amount of alkyl or alkenyl side chains or cross linkages.

What remains puzzling is that the aliphatic-to-aromatic C–H ratio increase with an increase in flame temperature. In general, soot carbonization is expected to accelerate at higher temperatures. The carbonization process presumably graphitizes the soot and, thus, should lead to smaller aliphatic-to-aromatic C–H ratios at higher temperature flames. A plausible explanation can be rationalized by a recent proposal that nascent soot contains persistent free radicals, which are aromatic in nature. These free radicals serve as active sites on an aromatic surface for aliphatics to bind to [39]. It may be hypothesized that a higher temperature flame causes nascent soot to contain a larger number of these persistent free radical sites, leading to a greater aliphatic content.

4. Conclusions

Micro-FT-IR analysis of soot samples collected from a set of lightly sooting ethylene–oxygen–argon flames indicates that in nascent soot the number of aliphatic C–H bonds exceeds that of aromatic C–H. The aliphatic-to-aromatic C–H ratio was observed to increase with an increase in flame temperature. Coupled with the findings of TD-CITOF-MS, the current results suggest that the aliphatic components are in the form of alkyl, alkenyl side chains or cross linkages covalently bound to aromatic units in the soot material. The present conclusion is consistent with a range of observations made in several previous studies, which all point to the fact that nascent soot is rich in aliphatics (consequently is liquid-like) and has a C/H atomic ratio around unity.

Acknowledgements

AL acknowledges support by the National Aeronautics and Space Administration (Grant NNG06GE89G). The work at USC was supported by the Strategic Environmental Research and Developmental Program and the National Science Foundation (CBET 0651990). A part of the flame experiments and all of the FT-IR analyses were performed at EMSL, a national scientific user facility sponsored by the DOE's Office of Biological and Environmental Research and located at Pacific Northwest National Laboratory (PNNL). PNNL is operated by the US Department of Energy by Battelle Memorial Institute under Contract No. DE-AC06-76RL0 1830.

References

[1] L.B. Ebert, J.C. Scanlon, C.A. Clausen, *Energy Fuels* 2 (1988) 438–445.
[2] H.F. Calcote, *Combust. Flame* 42 (1981) 215–242.
[3] R.A. Dobbins, R.A. Fletcher, W. Lu, *Combust. Flame* 100 (1995) 301–309.
[4] R.A. Dobbins, *Aerosol Sci. Technol.* 41 (2007) 485–496.
[5] A. Ciajolo, B. Apicella, R. Barbella, A. Tregrossi, *Combust. Sci. Technol.* 153 (2000) 19–32.
[6] A. Ciajolo, R. Barbella, A. Tregrossi, L. Bonfanti, *Proc. Combust. Inst.* 27 (1998) 1481–1487.
[7] A. Tregrossi, R. Barbella, A. Ciajolo, M. Alfe, *Combust. Sci. Technol.* 179 (2007) 371–385.
[8] B. Apicella, R. Barbella, A. Ciajolo, A. Tregrossi, *Chemosphere* 51 (2003) 1063–1069.
[9] A. D'Anna, Combustion generated fine carbonaceous particles, in: H. Bockhorn, A. D'Anna, A.F. Sarofim, H. Wang (Eds.), Proceedings of an International Workshop Held in Villa Orlandi, Anacapri (May 13–16, 2007), Karlsruhe University Press, Karlsruhe, 2009, pp. 289–320.
[10] B. Zhao, K. Uchikawa, H. Wang, *Proc. Combust. Inst.* 31 (2007) 851–860.
[11] A.D. Abid, N. Heinz, E.D. Tolmachoff, D.J. Phares, C.S. Campbell, H. Wang, *Combust. Flame* 154 (2008) 775–788.
[12] A.C. Barone, A. D'Alessio, A. D'Anna, *Combust. Flame* 132 (2003) 181–187.

[13] A.D. Abid, E.D. Tolmachoff, D.J. Phares, H. Wang, Y. Liu, A. Laskin, *Proc. Combust. Inst.* 32 (2009) 681–688.
[14] B.S. Haynes, H.G. Wagner, *Prog. Energy Combust. Sci.* 7 (1981) 229–273.
[15] B. Öktem, M.P. Tolocka, B. Zhao, H. Wang, M.V. Johnston, *Combust. Flame* 142 (2005) 364–373.
[16] H. Wang, A.D. Abid, Combustion generated fine carbonaceous particles, in: H. Bockhorn, A. D'Anna, A.F. Sarofim, H. Wang (Eds.), Proceedings of an International Workshop held in Villa Orlandi, Anacapri (May 13–16, 2007), Karlsruhe University Press, Karlsruhe, 2009, pp. 367–384.
[17] M.M. Maricq, *J. Aerosol Sci.* 40 (2009) 844–857.
[18] Y. Bouvier, C. Mihesan, M. Ziskind, et al., *Proc. Combust. Inst.* 31 (2007) 841–849.
[19] J.T. McKinnon, E. Meyer, J.B. Howard, *Combust. Flame* 105 (1996) 161–166.
[20] A. Santamaría, F. Mondragón, A. Molina, N.D. Marsh, E.G. Eddings, A.F. Sarofim, *Combust. Flame* 146 (2006) 52–62.
[21] A. Santamaria, F. Mondragon, W. Quinonez, E.G. Eddings, A.F. Sarofim, *Fuel* 86 (2007) 1908–1917.
[22] J.P. Cain, P.L. Gassman, H. Wang, A. Laskin, Micro-FTIR study of soot chemical composition – evidence of aliphatic hydrocarbons on nascent soot surfaces, *Phys. Chem. Chem. Phys.* 12 (2010) 5206–5218.
[23] N.P. Ivleva, A. Messerer, X. Yang, R. Niessner, U. Poschl, *Environ. Sci. Technol.* 41 (2007) 3702–3707.
[24] M. Frenklach, H. Wang, *Proc. Combust. Inst.* 23 (1991) 1559–1566.
[25] M. Frenklach, H. Wang, *Soot formation in combustion: mechanisms and models of soot formation*, in: H. Bockhorn (Ed.), *Springer Series in Chemical Physics*, vol. 59, Springer-Verlag, Berlin, 1994, pp. 162–190.
[26] M. Frenklach, *Phys. Chem. Chem. Phys.* 4 (2002) 2028–2037.
[27] B. Zhao, Z.W. Yang, J.J. Wang, M.V. Johnston, H. Wang, *Aerosol Sci. Technol.* 37 (2003) 611–620.
[28] B. Zhao, Z.W. Yang, Z.G. Li, M.V. Johnston, H. Wang, *Proc. Combust. Inst.* 30 (2005) 1441–1448.
[29] B. Zhao, Z.W. Yang, M.V. Johnston, et al., *Combust. Flame* 133 (2003) 173–188.
[30] D.J. Phares, S. Collier, *Aerosol Sci. Technol.* 44 (2010) 173–181.
[31] S.C. Wang, R.C. Flagan, *Aerosol Sci. Technol.* 13 (1990) 230–240.
[32] V.A. Marple, K.L. Rubow, S.M. Behm, *Aerosol Sci. Technol.* 14 (1991) 434–446.
[33] V.A. Marple, B.A. Olson, *A Micro-orifice Impactor with Cut Sizes Down to 10 Nanometers for Diesel Exhaust Sampling*, PTL Publication 113, Generic Technology Center for Respirable Dust, 1999.
[34] Y. Liu, Z.W. Yang, Y. Desyaterik, et al., *Anal. Chem.* 80 (2008) 7179.
[35] H. Jung, D.B. Kittelson, M.R. Zachariah, *Combust. Flame* 136 (2004) 445–456.
[36] Z.G. Li, H. Wang, *Phys. Rev. E* 68 (2003) 061206.
[37] Z.G. Li, H. Wang, *Phys. Rev. E* 68 (2003) 061207.
[38] A.D. Abid, J. Camacho, D.A. Sheen, H. Wang, *Combust. Flame* 156 (2009) 1862–1870.
[39] E. Dames, B. Sirjean, H. Wang, *J. Phys. Chem. A* 114 (2010) 1161–1168.